Biomaterials Advances 151 (2023) 213474

Contents lists available at ScienceDirect

Biomaterials Advances

journal homepage: www.journals.elsevier.com/materials-science-and-engineering-c

Biomineralization: A new tool for developing eco-sustainable Ti-doped hydroxyapatite-based hybrid UV filters

Elisabetta Campodoni [a,*], Margherita Montanari [a], Chiara Artusi [a], Linda Bergamini [a], Giada Bassi [a], Elena Destro [b], Ivana Fenoglio [b], Silvia Panseri [a], Anna Tampieri [a], Alessandra Sanson [a], Monica Sandri [a,*]

[a] Institute of Science and Technology for Ceramics-National Research Council (ISTEC-CNR), Faenza, Italy
[b] Department of Chemistry, University of Turin, Via Pietro Giuria 7, 10125 Turin, Italy

ARTICLE INFO

Keywords:
Biomineralization
Eco-sustainability
Physical filters
Biomimetic materials
Photostability

ABSTRACT

It is well known that the prolonged exposure to UV radiation from sunlight can compromise human health and is particularly damaging to the skin, leading to sunburn, photo-aging and skin cancer. Sunscreen formulations containing UV-filters present a barrier against solar UV and help to mitigate the harmful effects however, concern about their safety for both human and environmental health is still a much-debated topic. EC regulations classify UV-filters depending on their chemical nature, particle size, and mechanism of action. Furthermore, it regulates their use in cosmetic products with specific limitations in terms of concentration (organic UV filters) and particle size and surface modification to reduce their photo-activity (mineral UV filters). The regulations have prompted researchers to identify new materials that show promise for use in sunscreens. In this work, biomimetic hybrid materials composed of titanium-doped hydroxyapatite (TiHA) grown on two different organic templates, derived from animal (gelatin - from pig skin) and vegetable (alginate - from algae) sources. These novel materials were developed and characterized to obtain sustainable UV-filters as a safer alternative for both human and ecosystem health. This 'biomineralization' process yielded TiHA nanoparticles that demonstrated high UV reflectance, low photoactivity, good biocompatibility and an aggregate morphology which prevents dermal penetration. The materials are safe for topical application and for the marine environment; moreover, they can protect organic sunscreen components from photodegradation and yield long-lasting protection.

1. Introduction

Sunlight is essential for human health. It is responsible for internal clock regulation, metabolism stimulation, hormonal and immune system modulation. However, high levels of UVA and UVB in sunlight provoke negative health effects such as photo-aging, sunburn (erythema), dermatitis, immune suppression and ultimately photocarcinogenesis in the forms of carcinoma and melanoma [1,2]. A common strategy to mitigate these conditions is to apply sunscreen before sun exposure. Correctly formulated sunscreens normally contain active ingredients to filter incident UV radiation, excipients to ensure a comfortable feel on the skin and anti-oxidants to ensure shelf-life and stability. These components are formulated as either oil-in-water or water-in-oil emulsions, often incorporating high molecular weight esters to optimize viscosity [2].

Among the UV radiation given off by the sun, UVC (100–290 nm) is completely absorbed by oxygen molecules in the stratosphere (ozone-oxygen cycle) and UVB (290–320 nm) is partially absorbed by the ozone. The remaining UVA radiation (320–400 nm) and a minimal part of UVB reach the skin provoking metabolic and biological reactions [3].

According to EC Regulation No. 1223/2009, UV filters allowed in cosmetic formulations are classified based on their chemical composition and mechanism of action in organic (also chemical) or inorganic (also physical) UV filters [1,4,5]. Organic filters are usually aromatic compounds able to absorb UV radiation energy, releasing it as heat or radiation at a higher wavelength. Although they are cost effective, easily formulated and provide good 'skin feel', several are photo-unstable, degrading to non-UV absorbing products which decreases the efficiency of the sunscreen and leading to toxicological concerns for both human and environmental health [6–8]. In particular, as a recent review

* Corresponding authors.
E-mail addresses: elisabetta.campodoni@istec.cnr.it (E. Campodoni), monica.sandri@istec.cnr.it (M. Sandri).

https://doi.org/10.1016/j.bioadv.2023.213474
Received 25 November 2022; Received in revised form 10 May 2023; Accepted 12 May 2023
Available online 15 May 2023

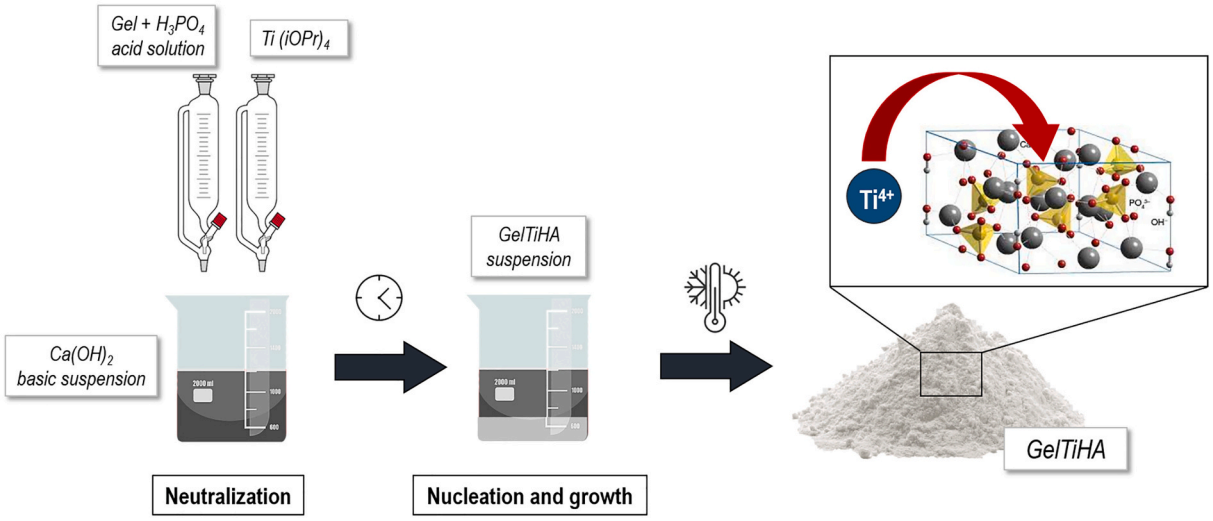

Fig. 1. Schematic representation of GelTiHA synthesis.

by Narla et al. [9] reported, the main problem linked to their use is their lipophilic property which often determines their penetration into the skin, furthermore, the tendency to photochemically degrade, generates free radicals which cause phototoxic reactions and skin irritation [2,9–11]. Furthermore, their long-term persistence in the marine environment at ppb concentrations provokes irreversible damage to the ecosystem, such as coral bleaching, which led several governments (Palau, Thailand, Philippines, Mexico, Florida, Virgin Island, and Hawaii) to ban some of them [12]. According to COSMOS [13] their use in cosmetic products is prohibited, however, a recent opinion of SCCS states that they can be considered but limited within a specific range of concentration [14].

Physical filters, on the other hand, are mineral, inorganic or composite (coated) particles that provide UV-shielding through absorption, reflection and scattering properties largely depending on their particle size (e.g. absorption mechanism is prevalent in nano-particles) and offer an alternative to the organics. Among the largely used physical filters are zinc oxide (ZnO) and titanium dioxide (TiO_2) [1,2,15], which are allowed at the maximum concentration of 25 % according to EC regulation no. 1223/2009 [5]. TiO_2 is mostly a UVB filter, but it can also act as a UVA filter depending on its particle size, and thus suitable to prepare a formulation with high-SPF without the requirement of additional filters. ZnO is less efficient due to lower UVB shielding, whereas has a broader profile in the UVA range and a lower refractive index which gives more transparency to formulations than TiO_2. TiO_2 above 200 nm in size, can reflect also visible light resulting in an unpleasant whitening effect in sunscreen. This effect has been overcome by reducing the particles' size below 100 nm, conversely, the nano-sized particles, despite improving sunscreen texture, increase the risk of deeper skin layer penetration, causing toxic reactions and skin irritation [16–18].

When TiO_2 is photo-excited, it generates reactive oxygen species (ROS) able to oxidize and degrade the other formulation ingredients, as well as harming the environment once released in water, raising unquestionable safety concerns [19,20]. Two different crystalline forms are possible for TiO_2, anatase and rutile, which have different photocatalytic activity [20]. Anatase is often used for water and air purification or photodynamic treatment of cancer due to its pronounced photocatalytic activity and, consequently, it should be avoided in sunscreen formulations. On the other hand, rutile is less, but still photoreactive [20]. Despite these issues, COSMOS, in a communication of August 2016, reported that ZnO and TiO_2 are the only alternatives to petrochemical UV filters in terms of efficacy and safety. In addition, EC regulation no. 1223/2009 now restricts their use in cosmetics by specifying that the number of particles with size below 100 nm must be <50 % and that the mass fraction below 100 nm constitutes <10 % of the total mass [5,13].

Recent studies developed TiO_2 nanoparticles with decreased photocatalytic activity due to modification with organic or inorganic coating [21,22]. Despite this, was demonstrated that TiO_2 particles used in sunscreen are still photoactive and responsible for damaging cultured human skin [23], DNA plasmids and cultured human skin fibroblasts [24].

For these reasons, there is an urgent need of developing safer and more effective solar filters. This work addressed this issue by engineering an active material as a UV filter, with composition and particle size that fulfil the formulation requirements and environmental and human safety concerns [25–27].

Given the growing interest of the last decade in calcium phosphates (CaPs) based compounds, especially hydroxyapatite (HA), the main component of hard human connective tissues, used in the most diverse applications, such as bone tissue engineering, nanomedicine and cosmetic [28], due to its excellent biocompatibility, biomimicry and versatility [21,29–31], we aimed here to create an innovative physical UV filter based on it.

A bioinspired in-lab biomineralization process was employed to nucleate nanostructured hydroxyapatite (nano-HA) crystals directly onto an organic natural matrix, obtaining hybrid particles where the nano-HA is confined and linked to the organic molecules, and endowed with UV shielding properties thanks to the titanium ions doping [32–34].

Two natural organic matrices, alginate (Alg), a polysaccharide derived from brown algae [35], and gelatin (Gel), a collagen-derived polypeptide [36], were selected to obtain two types of hybrid material.

The first, GelTiHA, obtained by the biomineralization of Ti-doped HA onto Gel molecules, was developed looking upon the increasingly important concept of circular economy, being Gel a byproduct of the food industry. The second, AlgTiHA, obtained by following an analogous process involving Alg molecules, was developed considering the preference of cosmetic industries for ingredients plant-derived rather than animal-derived.

Both compounds were compared in terms of performance to a commercial physical solar filter (Solaveil™). They are shown to be effective solar filters, with no photo-catalytic effect and harmless degradation products. They emerge as highly promising 'green', eco-sustainable physical UV filters, and viable alternatives for the development of safe and efficient sunscreen formulations.

2. Materials & methods

2.1. Chemicals and reagents

Gelatin (Gel) with mesh 4 and bloom 280 extracted from pig skin was purchased from Italgelatine (Cuneo, Italy). Alginic acid sodium salt (Alg) from brown algae, phosphoric acid (H_3PO_4, 85 wt%), calcium hydroxide ($Ca(OH)_2$, 95 wt%), titanium (IV) isopropoxide ($Ti(iOPr)_4$, 97 wt%) and isopropanol (C_3H_8O) were purchased from Sigma Aldrich, (USA). Commercial standard (Solaveil™ XTP1), composed of titanium dioxide (80 wt%), stearic acid and alumina in form of round nanoparticles with a diameter of about 50 nm, were purchased from Croda (UK).

2.2. Synthesis process

2.2.1. GelTiHA synthesis

Heterogeneous nucleation of TiHA nanocrystals on assembling Gel matrix was realized through a neutralization reaction performed as follows (Fig. 1). A Gel solution (3.32 g of gel in 83 mL H_2O at 45 °C) was mixed with a phosphate solution (3.46 g of H_3PO_4 in 30 mL H_2O) to obtain an acid solution. Meanwhile, a titanium solution was prepared by adding 2.20 g of Ti-$(iOPr)_4$ dropwise to 15 mL of isopropanol under argon flux to eliminate moisture and avoid TiO_2 formation. Finally, a basic suspension was obtained by dispersing 3.90 g of $Ca(OH)_2$ in 100 mL of H_2O at 45 °C under mechanical stirring for 30 min. In a three-necked round bottom flask the basic solution, maintained at 45 °C, was vigorously mechanically stirred. Two dropping funnels, containing the gel/phosphoric acid solution and titanium isopropoxide solution respectively, were attached to the flask, and these solutions were added dropwise and simultaneously to the basic solution. During the addition, the gradual formation of a white precipitate was observed. After the addition of the two reagents was completed, stirring at 45 °C was continued for 2 h, the flask was then left to rest at room temperature for a further hour. The product was centrifuged at 11,000 rpm for 10 min. The resulting pellet was washed with double-distilled water by resuspension and centrifugation 3 further times before freeze-drying.

A controlled freeze-drying process was applied, setting the cooling temperature at −40 °C and the heating ramp at 5 °C min^{-1} up to −5 °C and 2 °C min^{-1} up to 15 °C, under a pressure of 0.086 mbar until the obtainment of a dried white powder.

2.2.2. AlgTiHA synthesis

Heterogeneous nucleation of TiHA nanocrystals on assembling Alg matrix was realized through a neutralization reaction performed as follows (Fig. 2). A basic suspension of $Ca(OH)_2$ (4.72 g of $Ca(OH)_2$ in 100 mL H_2O) and a phosphate solution (4.15 g of H_3PO_4 in 30 mL H_2O) were prepared. Meanwhile, a titanium solution was prepared by adding 2.20 g of Ti-(iOPr)4 dropwise to 15 mL of isopropanol under argon flux to eliminate moisture and avoid TiO_2 formation. In a three-necked round bottom flask the basic solution, maintained at 45 °C, was vigorously mechanically stirred. Two dropping funnels, containing the phosphoric acid solution and titanium isopropoxide solution respectively, were attached to the flask, and these solutions were added dropwise and simultaneously to the basic solution. Once finished the dripping, Alg solution (4 g of alginate in 100 mL H_2O) was slowly added to the mixture to avoid agglomerates formation. During the addition, the gradual formation of a white precipitate was observed. After the addition of all the reagents was completed, stirring at 45 °C was continued for 2 h, the flask was then left to rest at room temperature for a further hour. The product was centrifuged at 11,000 rpm for 10 min. The resulting pellet was washed with double-distilled water by resuspension and centrifugation 3 further times before freeze-drying.

2.3. Characterization methods

2.3.1. Scanning Electron Microscopy

Sample morphology was examined by Scanning Electron Microscopy (SEM). In particular, the equipment employed was a FEG-SEM (Field Emission Gun Scanning Electron Microscope, FEI, Quanta 200, USA) for high-resolution images at high magnification and ESEM (Environmental Scanning Electron Microscope, Quanta 600 FEG, FEI Company, Hillsboro, OR) for high-resolution images at low magnification. For both analyses, the specimens were previously mounted on aluminium stubs utilizing carbon tape and gold coated using a coating unit Polaron Sputter Coater E5100 (Polaron Equipment, Watford, Hertfordshire, UK). The dimensional analysis was performed through ImageJ software.

2.3.2. X-ray diffraction

The crystal structure of the composites was established by powder X-Ray Diffraction (XRD) analysis. The D8 Advance diffractometer model (Bruker, Karlsruhe, Germany) working with Bragg-Brentano configuration was employed, equipped with a LINXEYE position-sensitive detector (CuKα radiation, λ = 1.5418 Å) generated at 40 kV and 40 mA. The XRD patterns were recorded in the 2θ range 10°-80°, 0.02° scan step and 0.5 s step time. Secondary phase (TiO_2) presence was calculated by Rietveld refinement considering a multi-phase system, using tabulated atomic coordinates of HA and TiO_2 (HA: PDF card 00–009-0432, TiO_2: PDF card 00–088-1175) with TOPAS5 software.

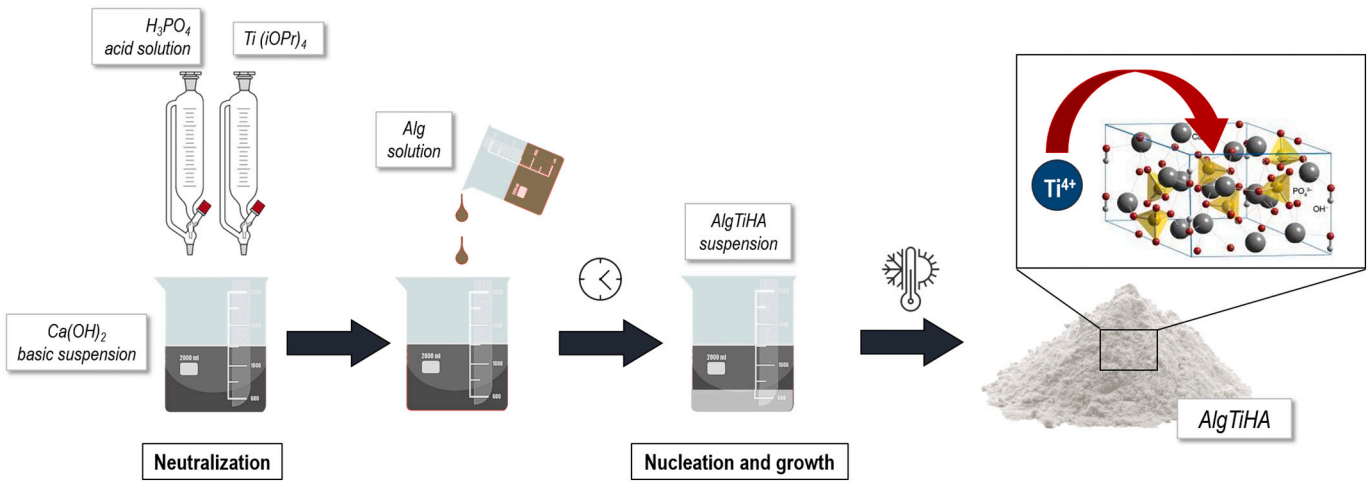

Fig. 2. Schematic representation of AlgTiHA synthesis.

2.3.3. Thermogravimetric analysis

The thermal behaviour of the composites was determined by Thermogravimetric Analysis (TGA) using the Simultaneous Thermal Analyzer (STA 409C, Netzsch, Germany). The experiment was performed within the 10–1100 °C temperature range, using a heating rate of 10 K/min under airflow. For the analysis, 20 mg of sample and an Al_2O_3 crucible were employed.

2.3.4. Fourier-transform infrared spectroscopy

The spectra were collected by Fourier-Transform Infrared Spectroscopy (FTIR) with a Thermo Nicolet-Avatar 320 FT-IR (Thermo Fisher Scientific Inc., Waltham, MA, USA). For the analysis, about 2 mg of the sample was finely ground with 100 mg of anhydrous potassium bromide (KBr) to remove scattering effects from large crystals, and then pressed at 8000 psi into 7 mm diameter disc to form a translucent pellet. All the spectra presented resulted from the average of 64 spectra, collected at room temperature in 400–4000 cm^{-1} wavelength range at the resolution of 4 cm^{-1}. Potassium bromide was used as a control.

2.3.5. Inductive coupled plasma optical emission spectroscopy

The chemical composition of the samples was obtained by Inductive Coupled Plasma Optical Emission Spectroscopy (ICP-OES). To perform the analysis an ICP-OES Liberty 200, Varian (Clayton South, Australia) was employed. Samples were prepared by dissolving 20 mg of each in 2 mL of nitric acid (HNO_3) and then making them up to 100 mL volume with deionized water after 30 min of sonication. Standard solutions of the element of interest were used as a reference and equally diluted in the solution of nitric acid as blank.

2.3.6. Ultraviolet-visible spectroscopy

Absorbance, reflectance and transmittance of the samples were recorded by Ultraviolet-Visible Spectroscopy (UV–Vis), using a UV–Vis-NIR spectrophotometer Lambda 750 (Perkin Elmer Instrument, USA). AlgTiHA and GelTiHA absorbance, reflectance and transmittance spectra were recorded from 280 to 700 nm and compared with one of the commercial references Solaveil™. For absorbance analysis, the powders were suspended in distilled water with a concentration of 10 mg L^{-1} and sonicated for 10 min with a sonicating probe, while for reflectance and transmittance, the powders were simply loaded on a sample holder.

2.3.7. Photodegradation test

Photoactivity tests were conducted by Rhodamine B (≥95 %, Sigma Aldrich) degradation under simulated sunlight. Into a refrigerated beaker, 50 mg of powder was dispersed in 60 mL of a 5 mgL-1 Rhodamine B solution and stirred in dark conditions for 30 min to allow Rhodamine B molecule absorption on the powder surface. The refrigerated beaker was irradiated by a solar simulator (ABET Technologies Sun 2000, Connecticut), previously calibrated with a Silicon reference cell at 1000 W m^2 AM 1.5. For each sample, 3 mL aliquots of suspension were removed after 0, 15, 30, 60, 90 and 120 min and after centrifugation at 5000 rpm for 1 min to separate the powder from the dye solution each aliquot was analyzed by the UV–Vis-NIR spectrophotometry. TiO_2 Aeroxide P25 (Evonik Industries, Germany), was used as the positive control. Analysis was performed in three replicates [34].

2.3.8. Generation of reactive oxygen species

Reactive oxygen species (ROS) generation was evaluated by X-Band EPR spectroscopy (Miniscope 100 EPR spectrometer, Magnettech, Berlin, Germany). Instrument settings were microwave power 7 mW, modulation amplitude 1G, scan time 80 s, and two scans.

Samples were irradiated with a 500 W mercury/xenon lamp (Oriel Instruments) equipped with an IR water filter to avoid suspension overheating and a 400 nm cut-off filter. Light irradiance, measured with a photo-radiometer (Delta Ohm S. r. L., Padova, Italy) was set to 518.5 W m^{-2} (1050–400 nm, NIR-vis) and 67.8 × 10^{-3} W m^{-2} (400–315 nm, UVA).

For evaluating the reactivity with sodium formate, 20 mg of samples powder were suspended in 0.5 mL of buffer solution (Phosphate Buffered Saline (PBS) 6 mM, pH 7.4) containing DMPO (72 mM) and sodium formate (1 M) and the suspension maintained under illumination in constant stirring in a quartz vial. The EPR spectra were recorded on 50 μL of the sample after 60 min from the reaction start.

For singlet oxygen formation, 20 mg of samples powder were suspended in 2 mL of a 50 mM solution of 4-oxo-TMP (2,2,6,6-tetramethyl-4-piperidone, Sigma-Aldrich) in PBS (10 mM, pH 7.4) and the suspension maintained under illumination in constant stirring in a quartz vial. The EPR spectra were recorded on 50 μL of the sample after 60 min from the reaction start.

As negative controls, in all the experiments, the same solutions not containing the samples and illuminated at the same conditions were employed. TiO_2 Aeroxide P25 (Evonik Industries, Germany), was used as the positive control. Analysis was performed in two replicates.

2.3.9. Cell culture

BALB/3 T3 murine fibroblast (Clone A31, ATCC® CCL-163™) were cultured in high glucose with pyruvate Dulbecco's Modified Eagle's Medium (DMEM) (Gibco) supplemented with 10 % Calf Bovine Serum (CBS, Gibco) and 1 % penicillin-streptomycin solution (100 U/ml-100 μg/mL, Gibco), kept at 37 °C under 5 % CO_2 atmosphere conditions and controlled humidity. Cells were detached from the culture flask by trypsinization and centrifuged. The cell number and viability were defined by the Trypan Blue Dye Exclusion test.

AlgTiHA, GelTiHA and Solaveil disks with a final dimension of 15 of diameter × 2 mm height were obtained by pressing 0.5 g of each powder for 60 s at 110 mbar (CCR Nannetti, A/84) and sterilized by 25 kGy gamma-ray radiation before use. They were pre-conditioned for 24 h in complete culture media before seeding 80.000 cells/sample by carefully dropping 30 μl cell suspension on the sample's upper surface. After 30 min-incubation at 37 °C which allows a preliminary cell adhesion, 1.5 ml of complete culture media was added to each sample and gently changed after 3 days. Cell cultures were kept at 37 °C with 5 % CO_2 atmosphere and controlled humidity conditions up to 7 days. All cell-handling procedures were performed under biological laminar-flow hood and sterility conditions.

2.3.10. Cell viability analysis

Quantitative cell viability analysis was performed via MTT assay. Briefly, MTT reagent ([3-(4,5-dimethylthiazol-2-yl)-2,5-diphenyltetrazolium bromide] (Sigma) was dissolved in PBS 1× at a concentration of 5 mg/mL. At each culture time point (1, 3 and 7 days), the samples were incubated with 10 % well-volume MTT solution for 2 h at 37 °C. The culture medium was then removed and substituted by Dimethyl Sulfoxide (DMSO), to dissolve insoluble formazan crystals derived from MTT conversion by living cells' metabolism. After 15 min of incubation under slight stirring conditions, each supernatant was transferred to a 96 well-plate in triplicate (200 μL/well) and the absorbance was read at 570 nm by Multiskan FC Microplate Photometer (Thermo Scientific). The absorbance values report in a directly proportional way to the alive cells' number. For each type of material, three samples were analyzed at each time point.

Qualitative cell viability and cytotoxicity analysis of the samples was performed via Live/Dead Assay for its ability to discriminate live from dead cells by simultaneously staining the esterase activity and the loss of plasma membrane integrity, respectively. At day 1 of culture, Live/Dead Assay (Live/Dead Assay Kit, Invitrogen) was performed according to manufacturer instructions. In brief, the samples were washed in PBS 1× and incubated in Live/Dead solution composed of PBS 1×, Acetoxymethyl Calcein (AM-calcein) 2 μM and Ethidium homodimer-1 (EthD-1) 4 μM for 15 min at 37 °C in dark conditions. Samples were washed and rinsed in PBS 1×. The image acquisition was performed by an inverted Ti-E fluorescence microscope (Nikon). For each type of material, one sample was analyzed.

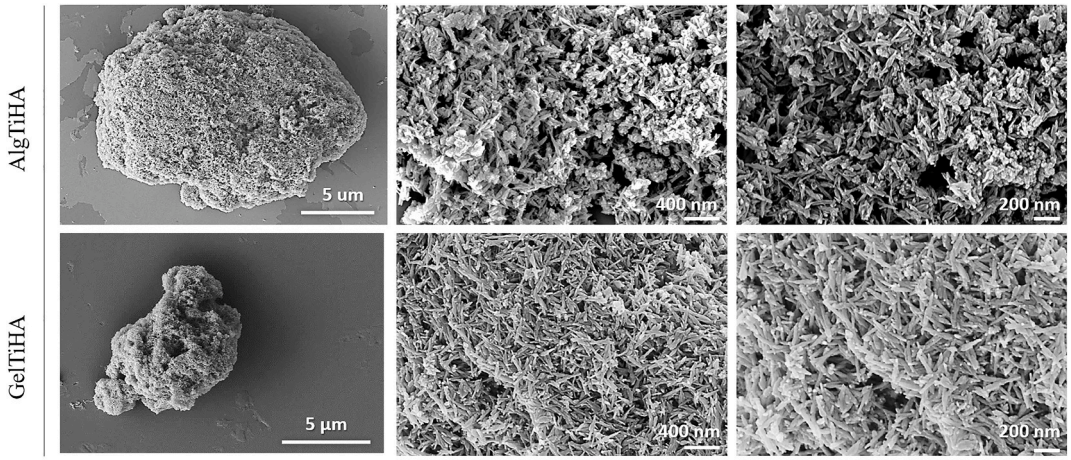

Fig. 3. SEM-FEG images of AlgTiHA and GelTiHA hybrid particles.

2.3.11. Cell morphology evaluation

Qualitative fluorescent detection of cell actin filaments and nuclei was performed at day 3 of the culture. Samples were washed in PBS 1× and fixed in 4 % (*w/v*) paraformaldehyde (PFA) (Sigma) for 15 min. The samples were then permeabilized in PBS 1× with 0.1 % (*v*/v) Triton X-100 for 15 min at room temperature, and incubated with FITC-conjugated fluorescein-phalloidin (38 nM, Invitrogen) (Faulstich et al., 1988). Samples were washed with PBS 1× for 5 min and incubated with nuclear stain 4′-6-Diamidino-2-phenylindole (DAPI) (Invitrogen) 300 nM in PBS 1× per 5 min. The images were acquired by an inverted Ti-E fluorescence microscope (Nikon). For each type of material, one sample was analyzed.

A further evaluation of cell morphology and cell-material interaction was performed by Scanning Electron Microscope (SEM) analysis at day 3 of culture. Briefly, the samples were washed in 0.1 M Sodium Cacodylate Buffer pH 7.4 and fixed in 2.5 % Glutaraldehyde (Sigma) in 0.1 M Sodium Cacodylate Buffer pH 7.4 for 2 h at 4 °C. After washings in 0.1 M Sodium Cacodylate Buffer pH 7.4, the samples were dehydrated in a graded series of ethanol followed by Hexamethyldisilazane reagent (HMDS ≥99 %, Sigma). For the analysis, the samples were sputter-coated with 20 µm of gold film. For each type of material, one sample was analyzed under high vacuum conditions by SEM (ESEM Quanta 200, FEI).

2.3.12. Statistical analysis

Statistical analysis of MTT data was performed by GraphPad Prism software (version 6.0). The results were reported in the graph as mean ± standard error of the mean and they were analyzed by two-way analysis of variance (two-way ANOVA) followed by Dunnett's multiple comparison test compared to Solaveil control.

3. Results & discussion

The synthesis of Ti-doped HA nanocrystals on Gel and Alg biopolymer matrices to obtain the hybrid particles, occurred by reproducing the natural biomineralization process in which the multiple sequential steps, specifically the nucleation, crystallization, and growth of TiHA nanoparticles, were strongly influenced by the presence of the polymeric matrices, which played the role of crystallization inhibitors.

Analogously to what occurs in the previously investigated laboratory-scale biomineralization of collagen [32,33], Gel molecules guided the heterogeneous nucleation of low-crystalline TiHA nanoparticles through a neutralization method. For the obtainment of GelTiHA, the final pH of the suspension obtained after the synthesis was modified up to neutral value, at which the growth of the mineral particles on the Gel molecules could take place thanks to the bond of the calcium ions with the carboxylic groups exposed by Gel molecules.

Differently, to obtain the AlgTiHA, since both acid and basic environments would induced the alginate gelation [34,37], the Alg solution was poured in the reaction flask immediately after the conclusion of the neutralization reaction between the phosphoric acid and the titanium solutions added to the alkaline calcium hydroxide suspension. In this case the well noted high reactivity of Alg molecules with Ca(II) ions guaranteed the strong interaction between the mineral nano-particles and the organic matrix with the formation of the hybrid AlgTiHA particles.

Both hybrid particles, obtained through these bio-inspired processes, were compared with one of the most employed commercial physical UV filters, the Solaveil, of which these new eco-sustainable mineral particles are potential substitutes, capable of guaranteeing the sun protection properties without showing any toxicity for humans and for the marine environment [38].

Unlike collagen, one of the biopolymers better known for being involved in the biomineralization process, Gel and Alg are not featured by the tendency of collagen to self-assemble into 3D macromolecular fibrous structures, leading, after the biomineralization process, to the formation of mineralized hybrid particles characterized from a high percentage of mineral phase. This outcome is favoured by the involvement of most of their exposed functional groups in the interaction with calcium and phosphate ions, which increase the mineralization rate preventing the formation of three-dimensional structures [32,39,40]. The obtained hybrid particles morphology was proved through SEM-FEG (Fig. 3) analysis; both GelTiHA and AlgTiHA samples showed needle-like particles of, respectively, 304 ± 55 nm and 267 ± 76 nm in length ($n = 30$), with a slightly higher tendency to aggregate for AlgTiHA particles.

Needle-like particles are indeed reported in the literature as possible to induce a cytokines-mediated inflammatory response, which can consequently determine the cytotoxicity of the material. In particular, the needle-like morphology is highlighted as potentially cytotoxic due to the risk of this shape breaking cell membrane and leading to their death [41]. Nevertheless, a recent document issued by the Scientific Committee on Consumer Safety [42] has also made clear that the particle rod shape is the most suitable for cosmetic use since it is less dangerous for the skin. It must be highlighted that both AlgTiHA and GelTiHA, despite the needle-like morphology, are not inorganic single dispersed particles but hybrid materials, with the inorganic phase strictly linked to the organic matrix, potentially limiting their penetration into the dermis and any possible derived toxic effect. This evaluation would be part of a more complex dossier that will be presented to the SCCS, supporting the safe use of hybrid HA in cosmetic products [42].

XRD profiles showed the presence of a pure crystalline phase that can

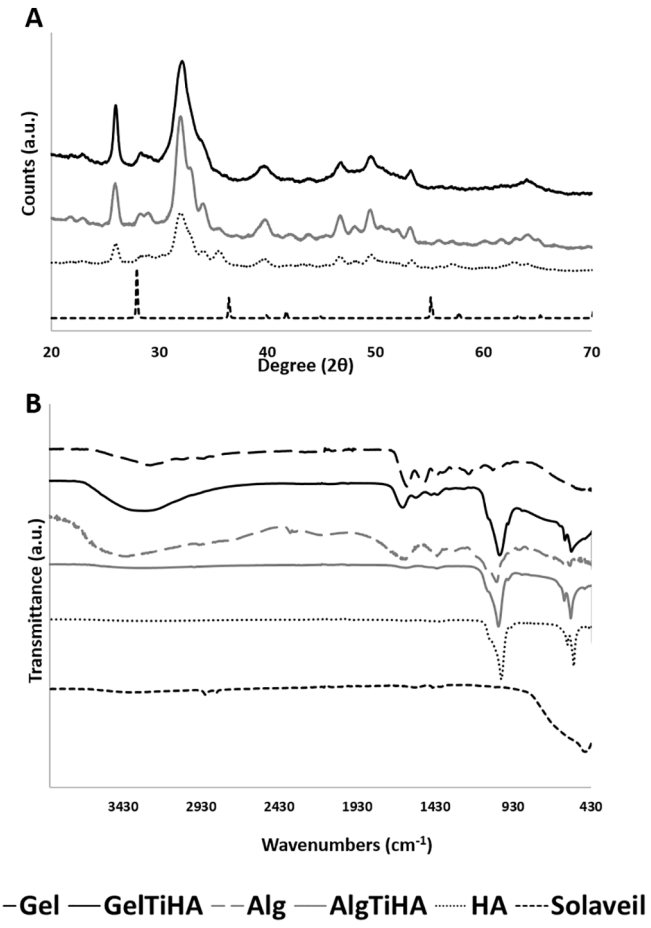

Fig. 4. A) XRD spectra and B) FTIR spectra of AlgTiHA and GelTiHA hybrid composites in comparison with Gel, Alg, HA and Solaveil™.

be identified as HA according to the PDF card #09–0432 (Fig. 4A). Both XRD patterns are poorly resolved and with low intensity, typical of mineral phases with a low degree of crystallinity. The scarce crystallinity might be ascribed to various factors. First, the low synthesis temperature hampered the formation of highly crystalline structures. Then, the presence of Gel and Alg directed the mineralization towards the formation of a low crystallinity phase, typical of the biomineralization process, in which the organic molecules act as nucleation templates for the mineral phase while hampering its growth [32,40]. Finally, the presence of titanium ions distorts the crystal lattice, thus leading to an intrinsically increased disordered crystal phase formation. No secondary crystalline phases were identified (e.g. TiO_2) through Rietveld analysis, highlighting as Ti ions are just present within the HA lattice or, in case, could be present as a secondary phase only in a highly amorphous state and in a quantity not detectable by the XRD analysis nor visible with SEM [38].

Observing the XRD spectra of the TiO_2 commercial sample (Solaveil™), the XRD pattern is in agreement with standard peaks of the rutile TiO_2 phase in PDF card #21–1276. The main peak is at 27°, which corresponds to (110) plane according to the TiO_2 anatase phase and (101) plane at 36°, as well as, (211) plane at 54°. No peaks of the anatase phase were revealed; this is consistent with the literature which shows a more photoreactivity of anatase than the rutile phase leading to more harmful particles for the cosmetic field [43].

FTIR analysis of GelTiHA and AlgTiHA revealed a similar pattern (Fig. 4B) showing peaks at 1036, 602, and 562 cm^{-1}. The signal at 1036 cm^{-1} corresponds to HA asymmetric stretching of PO_4 groups, while, peaks at 602 and 562 cm^{-1} are related to the bending of PO_4 groups. In AlgTiHA, only peaks related to the mineral phase are clearly visible

Table 1
Inorganic/organic ratio and chemical composition of GelTiHA and AlgTiHA evaluated by TGA and ICP.

	HA: Pol ratio	Ca/P (mol)	Ti/Ca (mol)	Ti/P (mol)	Ca/(Ti + P) (mol)	(Ca + Ti)/P (mol)	(Ca + Ti)/(P + Ti) (mol)
GelTiHA	84:16	1,66 ± 0.01	0,15 ± 0.01	0,25 ± 0.01	1,33 ± 0.01	1,91 ± 0.01	1.53 ± 0.01
AlgTiHA	92:8	1,60 ± 0.03	0,14 ± 0.01	0,23 ± 0.01	1,30 ± 0.04	1,84 ± 0.01	1.49 ± 0.03

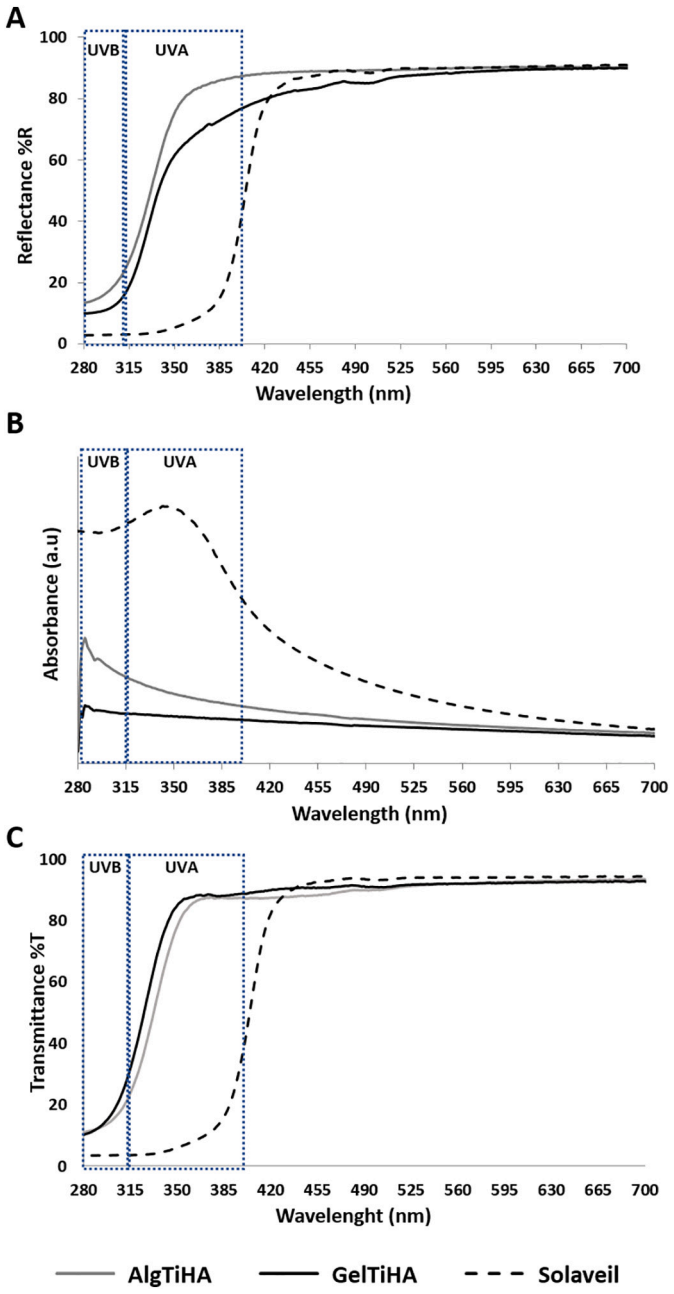

Fig. 5. A) Reflectance spectra; B) Absorption spectra and C) Transmittance spectra of AlgTiHA and GelTiHA hybrid composites in comparison with the commercial standard (Solaveil™).

probably due to the very high amount of hydroxyapatite fully covering the Alg molecules. Quite the opposite, in GelTiHA where a major amount of organic phase is present, also Gel peaks are clearly visible. In particular, the peak at 3405 cm^{-1} corresponds to the stretching vibrations of O—H bonds of Gel, while the peaks at 1650, 1547 and 1453 cm^{-1}, are related to the asymmetric and symmetric stretching vibrations of the carboxylate groups in Gel [40].

As mentioned above, the mineralization of Gel and Alg matrix allowed to obtain a high mineral content, confirmed by thermogravimetric analysis (TGA) that assessed the weight loss % at each temperature range, giving information on the hybrid HAs composition: content of water, organic fraction and mineral fraction (Table 1). TGA profiles revealed for both GelTiHA and AlgTiHA two different weight losses, the first, ranging from 20 °C to 150 °C, consisting of water loss, whereas the second, ranging from 150 °C to 800 °C, consisting of polymer degradation in line with literature reported [40,44,45]. The residual mass corresponds to the mineral component, TiHA, biomineralized on the two different biopolymers. In detail, GelTiHA ratio is more similar to the theoretical ratio (20:80), while the one of AlgTiHA is lower than 20:80, showing that less organic phase is present. This behaviour can be ascribable to the different biomineralization protocols (Alg was introduced after the neutralization process) and to the high affinity between Ca^{2+} ions and Alg, which favours the immediate interaction between the just formed hydroxyapatite and the alginate poured.

The chemical composition of the mineral phase was measured by ICP quantitative analyses in terms of the molar ratio between the elements (Table 1). Considering the evidence highlighted from XRD analyses, it was possible to assess the effective partial substitution of both Ca^{2+} ions and PO_4^{3-} ions in the HA lattice by, respectively, Ti^{4+} and TiO_4^{4-} ions, coherently with what was previously reported in the literature [38]. In particular, as expected, an increment of the (Ca + Ti) / *P* value compared to the Ca / P value was recorded, as well as a decrease in the Ca / (Ti + P) value. The small deviation of the Ca / *P* values from that of the pure HA (theoretical ratio 1.67) [46] can plausibly be attributed to a similar Ca^{2+} and PO_4^{3-} ions depletion by Ti^{4+} and TiO_4^{4-} ions.

UV–Vis spectroscopy is the best technique to determine the absorption and reflection properties of sunscreen composites. The reflection properties of the hybrid composites were reported in Fig. 5A. The reflectance profiles of both composites were very similar, GelTiHA and AlgTiHA revealed an area of middle values of reflectance between 280 and 320 nm followed by an increase of the reflectance value in the UVA range (315–400 nm) reaching a plateau of 90 % of reflectance at the edge of the visible range (400 nm). Comparing the reflection curves of the hybrid composites with a commercial sunscreen, it is clear how the reflectance values in the UVA and UVB (315–400 nm and 280–315 nm) range of Solaveil™ (TiO_2 based commercial sunscreen) are significantly lower (10 %) than GelTiHA and AlgTiHA, confirming, even more, the good reflection properties of these hybrid composites.

On the other hand, GelTiHA and AlgTiHA show lower absorption (Fig. 5B) than the commercial product: the curves decrease in an almost linear manner with the wavelength, while Solaveil presents an enhanced absorption, with a maximum peak at 350 nm to then decrease such as GelTiHA and AlgTiHA. This behaviour is likely due to the different particles size. While the hybrid particles synthesized are bigger than 200 nm, thus performing mainly as a physical blocker for the radiation, Solaveil™ particles, about 50 nm on average, act mainly as an inorganic UV absorber, as proven also by the lower transmittance compared to absorbance it shows in the UVA and UVB region (Fig. 5C). Despite using a different mechanism, both GelTiHA and AlgTiHA were nonetheless proven to be effective in shielding UVs radiations (Fig. 5) [47,48].

Finally, photodegradation tests of an aqueous solution of Rhodamine B were carried out exposing the system to a simulated full solar spectrum. No photocatalytic activity was detected by either AlgTiHA or GelTiHA under irradiation in comparison with the photo-catalyst Areoxide P25, used as the positive control. On the contrary, Solaveil™, showed photocatalytic activity, visible by the decrease of Rhodamine B

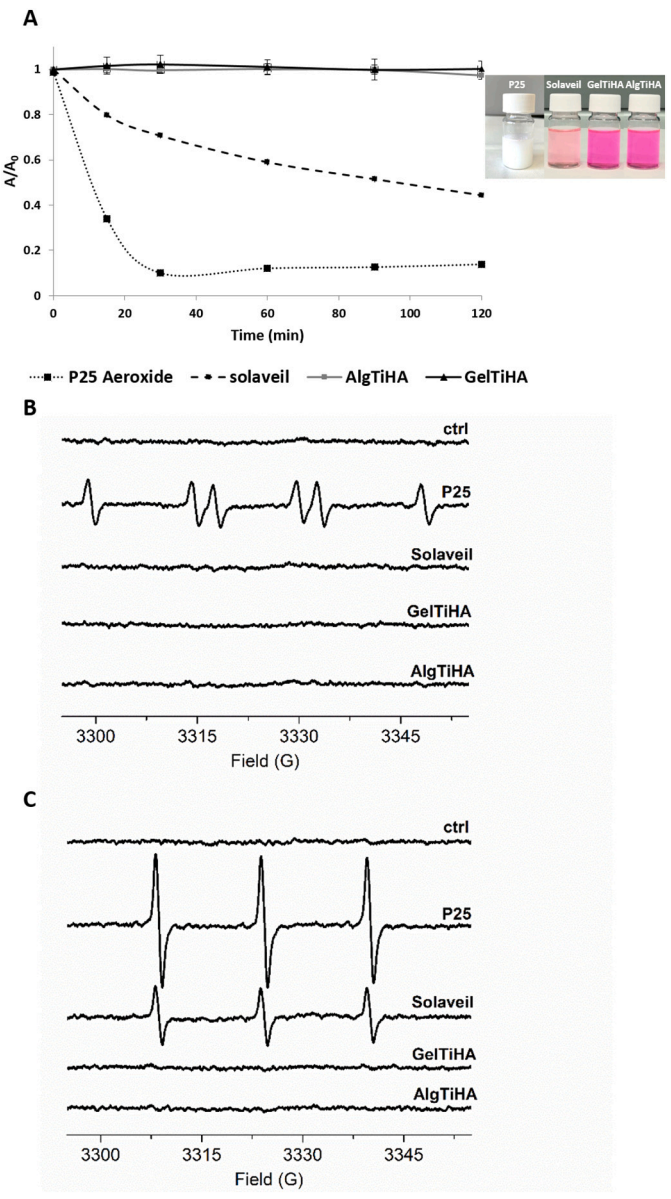

Fig. 6. Photoactivity of AlgTiHA and GelTiHA in comparison with Solaveil™and P25 as a control. A) degradation of Rhodamine and in the inset picture: Solaveil™, GelTiHA and AlgTiHA suspensions after simulated full solar spectrum irradiation in presence of Rhodamine B (5 mg/mL). B) Generation of carboxylate radicals by AlgTiHA and GelTiHA in comparison with Solaveil™and the photo-catalyst Areoxide P25. Representative EPR spectra were recorded after 60 min of samples irradiation in PBS solution (pH 7.4, DMPO) of sodium formate. The spectra correspond to the adduct DMPO-$COO^{\bullet-}$ C) Generation of singlet oxygen by AlgTiHA and GelTiHA in comparison with the commercial sample Solaveil and the photo-catalyst Areoxide P25. Representative spectra after 60 min of irradiation were generated in a solution of 4-oxo-TMP in PBS. The spectra correspond to the radical TEMPONE.

absorption maximum during the solar simulator time exposure. With Solaveil, >50 % of Rhodamine B was degraded in 120 min (Fig. 6A).

To dig deeper into this aspect of AlgTiHA and GelTiHA, their ability to generate Reactive Oxygen Species (ROS) was assessed by Electron Spin Resonance (EPR) spectroscopy. Titanium dioxide is known to generate several ROS (hydroxyl and superoxide radicals, hydrogen peroxide, singlet oxygen) as a consequence of UV light irradiation, that in turn can degrade organic molecules [49,50]. The generation of free radical species can be monitored by using formic acid as model organic molecule. In presence of free radical species, the carboxylate radical is

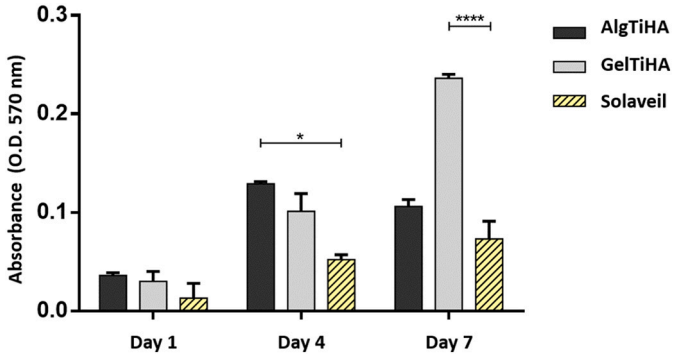

Fig. 7. Cell viability analysis by MTT test. The results were reported in the graph as mean ± error standard of the mean; *p value ≤0.05 and **** p value ≤0.0001.

formed and can be detected by EPR spectroscopy once stabilized by the spin trap DMPO [49]. Singlet oxygen can be detected by the probe 4-oxo-TMP. This molecule reacts specifically with singlet oxygen, leading to the formation of the stable radical TEMPONE.

In Fig. 6B and C the EPR spectra obtained with the AlgTiHA and GelTiHA are compared with those obtained with Solaveil and the photocatalyst Areoxide P25, used as the positive control [51].

In both tests, no signal was observed either for AlgTiHA or GelTiHA (Fig. 6B and C), thus confirming their inertness; on the other hand, the typical spectrum of TEMPONE radical was recorded for Solaveil™, indicating the production of singlet oxygen. The generation of this reactive specie confirmed the results previously obtained with the Rhodamine B test.

An in vitro cytotoxicity test using a common fibroblast cell line (BALB/3 T3 A31, ATCC® CCL-163™) was performed to assess the relative biocompatibilities of AlgTiHA, GelTiHA and the commercial Solveil™ product. Proliferation, performed by MTT assay, clearly showed significantly higher viability of cells cultured on both GelTiHA and AlgTiHA, demonstrating the absence of a cytotoxic effect. In detail, Fig. 7 showed a statistically significant increase in the proliferation of AlgTiHA (p values ≤0.05) and GelTiHA (p values ≤0.0001) samples at days 4 and 7 of culture, compared to Solaveil™. In addition, GelTiHA showed an increasing linear cell culture growth, differently from AlgTiHA, where a plateau in cell proliferation and no differences in cell viability were observed between day 4 and day 7 (Fig. 7). These results suggest Gel can perform better in terms of cell-material interaction, confirming the well-known intrinsic bioactivity of Gel on cell proliferation [52], compared to the relatively inert Alg [34,53].

The absence of cytotoxicity was also confirmed by a qualitative cell viability analysis performed with Live/Dead assay. Both GelTiHA and AlgTiHA samples did not compromise cell viability. At day 1, several live cells and very few dead cells were detected in both groups compared to the control group which showed higher cytotoxicity (Fig. 8A, B and C) confirming the quantitative cell viability results. It is important to notice that, 24 h after seeding, GelTiHA group showed also a more uniform cell distribution on the sample surface compared to the other two groups (Fig. 8A, B and C). Indeed, despite its biocompatibility, the biological inertness of Alg, together with its low bio-adhesivity, makes it less suitable for cell interaction and spreading as cells cannot establish specific attachment points with the polymer [54]. Conversely, Gel, due to its retention of collagen bioactive sequences, can create a more suitable microenvironment for cell adhesion [55], activating cell/surface processes that involve the reorganization of cytoskeleton proteins like actin [56]. In Fig. 8D, E and F, phalloidin stains actin filaments and a cell layer that covers the sample surface is evident in GelTiHA and AlgTiHA groups, compared to the control group where very few cells with irregular morphology are detectable at day 3 of culture. In detail, a more uniform cell layer is observed in GelTiHA, compared to AlgTiHA and the control group where empty zones on the material surface were found, confirming the qualitative analysis of cell viability (Fig. 8 D, E and F).

A further evaluation of cell morphology and interactions with the samples was also reported by SEM analysis at day 3 (Fig. 9). The SEM images confirmed the results detected with actin staining: overall, both AlgTiHA and GelTiHA showed a higher cell density compared to the Solaveil™ group (Fig. 9). Nevertheless, also SEM showed the presence of a more uniform cell layer on GelTiHA compared to AlgTiHA, confirming the previous viability and proliferation reported results.

4. Conclusion

A biomineralization synthesis process has been used to prepare two hybrid materials (GelTiHA and AlgTiHA) based on a Ti-doped hydroxyapatite mineral phase grown on biomolecules. Their nanostructure and the partial substitution of both Ca^{2+} and PO_4^{4-} with Ti^{4+} and TiO_4^{4-} ions within the HA lattice are responsible for their UV filtering properties. In addition, we propose that, since the Ti^{4+} ions are bound within

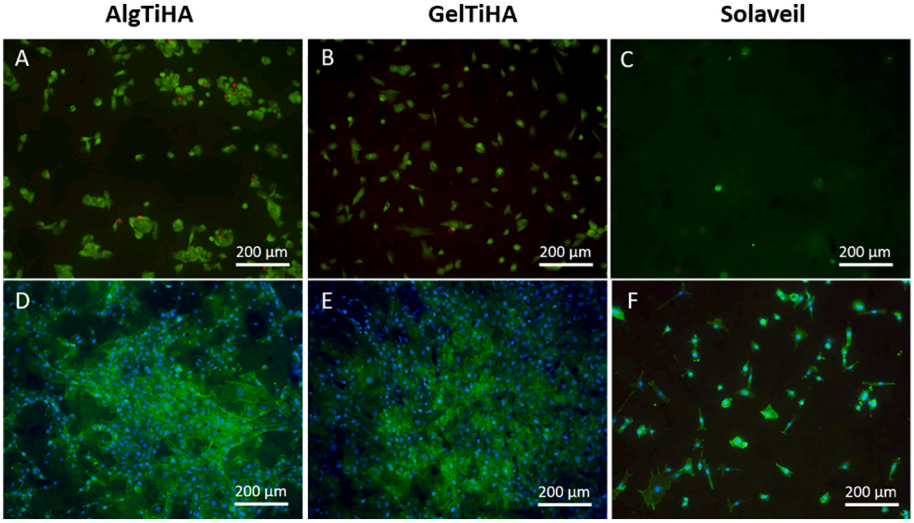

Fig. 8. A, B and C) Live/Dead Assay at day 1. Calcein stains live cells in green and Ethidium homodimer-1 stains dead cells in red; D, E and F) Cell morphology analysis at day 3. Fluorescein-phalloidin detection of actin filaments in green and DAPI detection of nuclei in blue. Scale bars are 200 µm. (For interpretation of the references to colour in this figure legend, the reader is referred to the web version of this article.)

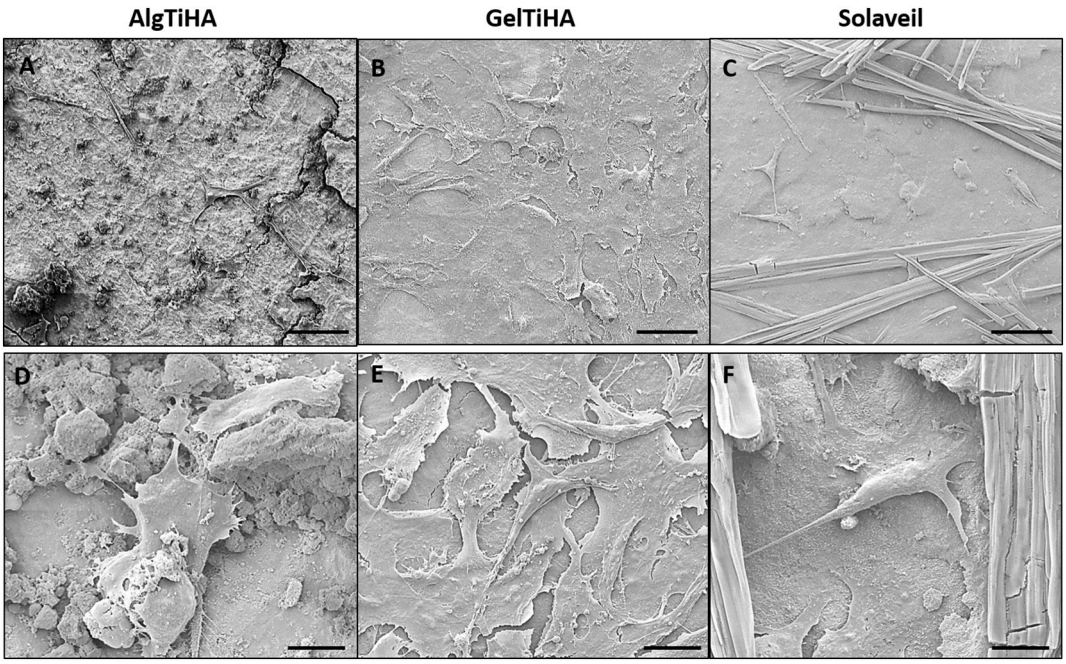

Fig. 9. SEM images of fibroblast cells cultured in contact with AlgTiHA (A, D), GelTiHA (B, E) and Solaveil™ (C, F) at day 3 of culture. Scale bars are 100 μm (A, B, C) and 20 μm (D, E, F).

the structure of HA crystals, this may be the underlying cause for the observed lack of photoactivity, which should reduce of the risk of sensitization during sun exposure.

The evidence reported here attests not only to the effectiveness of these materials as UV filters but also demonstrates their biocompatibility which should ensure enhanced human and ecosystem health compared to the ZnO and some of the TiO_2 UV filters widely used today in sunscreen formulations. Despite the nanometric size of the TiHA mineral particles, the organic matrices on which they are grown confine them in a hybrid micrometric structure, which reduces the potential risk of skin penetration.

These important features and behaviours make the materials highly prospective for the formulation of innovative, eco-sustainable sunscreen products endowed with increased safety and long-lasting protection.

CRediT authorship contribution statement

Elisabetta Campodoni: Conceptualization, performed the experiments, writing original draft, read and approved the final manuscript. Margherita Montanari: performed the experiments, writing original draft, read and approved the final manuscript. Chiara Artusi: performed the experiments, writing original draft, read and approved the final manuscript. Linda Bergamini: Performed the UV–vis spectroscopy and photodegradation experiment, writing original draft, read and approved the final manuscript. Giada Bassi: performed the biological experiments, writing original draft, read and approved the final manuscript. Elena Destro: Performed the EPR spectroscopy experiments, writing original draft, read and approved the final manuscript. Ivana Fenoglio: Conceptualized the EPR spectroscopy experiments, read and approved the final manuscript. Silvia Panseri: Conceptualized the biological experiments, read and approved the final manuscript. Alessandra Sanson: read and approved the final manuscript. Anna Tampieri: read and approved the final manuscript. Monica Sandri: Methodology, conceptualization, revised and approved the final manuscript.

Funding sources

This project has received funding from the Project PoC2020-ProtecTHA "Innovative UV filters for safer and more eco-sustainable sun protection" Co-financed from MiSE and CNR.

Declaration of competing interest

The authors declare that they have no known competing financial interests or personal relationships that could have appeared to influence the work reported in this paper.

Data availability

Data will be made available on request.

References

[1] C. Antoniou, M.G. Kosmadaki, A.J. Stratigos, A.D. Katsambas, Sunscreens – what's important to know, J. Eur. Acad. Dermatol. Venereol. 22 (2008) 1110–1119, https://doi.org/10.1111/j.1468-3083.2007.02580.x.

[2] M. Battistin, V. Dissette, A. Bonetto, E. Durini, S. Manfredini, A. Marcomini, E. Casagrande, A. Brunetta, P. Ziosi, S. Molesini, R. Gavioli, F. Nicoli, S. Vertuani, A. Baldisserotto, A new approach to UV protection by direct surface functionalization of TiO_2 with the antioxidant polyphenol dihydroxyphenyl benzimidazole carboxylic acid, Nanomaterials. 10 (2) (2020) 231, https://doi.org/10.3390/nano10020231.

[3] M.E. Burnett, J.Y. Hu, S.Q. Wang, Sunscreens: obtaining adequate photoprotection, Dermatol. Ther. 25 (2012) 244–251, https://doi.org/10.1111/j.1529-8019.2012.01503.x.

[4] F. Yu, W. Ruoyu, Y. Lei, X. Lidan, H. Junfei, T. Jie, H. Hailun, G. Zhipeng, L. Yiwen, Propolis inspired sunscreens for efficient UV-protection and skin barrier maintenance, Nano Res. 15 (2022) 8237–8246, https://doi.org/10.1007/s12274-022-4434-z.

[5] Regulation (EC) No 1223/2009 of the European Parliament and of the Council of 20 November 2009 on Cosmetic Products., (n.d.). https://eur-lex.europa.eu/eli/reg/2009/1223 (accessed February 27, 2023).

[6] A.N. Barone, C.E. Hayes, J.J. Kerr, R.C. Lee, D.B. Flaherty, Acute toxicity testing of TiO_2-based vs. oxybenzone-based sunscreens on clownfish (Amphiprion ocellaris), Environ. Sci. Pollut. Res. 26 (2019) 14513–14520, https://doi.org/10.1007/s11356-019-04769-z.

[7] S.L. Schneider, H.W. Lim, Review of environmental effects of oxybenzone and other sunscreen active ingredients, J. Am. Acad. Dermatol. 80 (2019) 266–271, https://doi.org/10.1016/j.jaad.2018.06.033.

[8] Y. Huang, J.C.F. Law, T.K. Lam, K.S.Y. Leung, Risks of organic UV filters: a review of environmental and human health concern studies, Sci. Total Environ. 755 (2021), 142486, https://doi.org/10.1016/j.scitotenv.2020.142486.

[9] S. Narla, H.W. Lim, Sunscreen: FDA regulation, and environmental and health impact, Photochem. Photobiol. Sci. 19 (2020) 66–70, https://doi.org/10.1039/c9pp00366e.

[10] T. Manasfi, B. Coulomb, S. Ravier, J.-L. Boudenne, Degradation of organic UV filters in chlorinated seawater swimming pools: transformation pathways and bromoform formation, Environ. Sci. Technol. 51 (2017) 13580–13591, https://doi.org/10.1021/acs.est.7b02624.

[11] G. Tortini, P. Ziosi, E. Cesa, S. Molesini, E. Baldini, D. De Lucia, C. Rossi, E. Durini, S. Vertuani, S. Manfredini, Criticisms in the development of high-protection and broad-spectrum "natural/organic" certifiable sunscreen, Cosmetics 9 (2022) 56, https://doi.org/10.3390/cosmetics9030056.

[12] M. Vieira Sanches, M. Oliva, L. De Marchi, A. Cuccaro, D. Puppi, F. Chiellini, R. Freitas, C. Pretti, Ecotoxicological screening of UV-filters using a battery of marine bioassays, Environ. Pollut. 290 (2021), 118011, https://doi.org/10.1016/J.ENVPOL.2021.118011.

[13] COSMOS-standard AISBL, COSMOS Position on the Mineral UV-filter in Organic and Natural Cosmetics. https://media.cosmos-standard.org/filer_public/30/ea/30ea5944-cf28-44ab-bec6-f4f7ca6c74f1/cosmos-standard_v31.pdf, 2020. (Accessed 27 February 2023).

[14] P.E. Bernauer U, Bodin L, Chaudhry Q, CoenraadsPJ, Dusinska M, Ezendam J, Gaffet E, Galli CL, Granum B, Octocrylene, (n.d.). https://health.ec.europa.eu/publications/octocrylene_en (accessed February 27, 2023).

[15] S.W.Y. Wong, G.J. Zhou, P.T.Y. Leung, J. Han, J.S. Lee, K.W.H. Kwok, K.M. Y. Leung, Sunscreens containing zinc oxide nanoparticles can trigger oxidative stress and toxicity to the marine copepod *Tigriopus japonicus*, Mar. Pollut. Bull. 154 (2020), 111078, https://doi.org/10.1016/j.marpolbul.2020.111078.

[16] N. Serpone, D. Dondi, A. Albini, Inorganic and organic UV filters: their role and efficacy in sunscreens and suncare products, Inorg. Chim. Acta 360 (2007) 794–802, https://doi.org/10.1016/j.ica.2005.12.057.

[17] N. Serpone, Sunscreens and their usefulness: have we made any progress in the last two decades? Photochem. Photobiol. Sci. 20 (2021) 189–244, https://doi.org/10.1007/s43630-021-00013-1.

[18] P.J. Lu, S.W. Fang, W.L. Cheng, S.C. Huang, M.C. Huang, H.F. Cheng, Characterization of titanium dioxide and zinc oxide nanoparticles in sunscreen powder by comparing different measurement methods, J. Food Drug Anal. 26 (2018) 1192–1200, https://doi.org/10.1016/j.jfda.2018.01.010.

[19] D. Hanigan, L. Truong, J. Schoepf, T. Nosaka, A. Mulchandani, R.L. Tanguay, P. Westerhoff, Trade-offs in ecosystem impacts from nanomaterial versus organic chemical ultraviolet filters in sunscreens, Water Res. 139 (2018) 281–290, https://doi.org/10.1016/j.watres.2018.03.062.

[20] L. Tiano, T. Armeni, E. Venditti, G. Barucca, L. Mincarelli, E. Damiani, Modified TiO_2 particles differentially affect human skin fibroblasts exposed to UVA light, Free Radic. Biol. Med. 49 (2010) 408–415, https://doi.org/10.1016/j.freeradbiomed.2010.04.032.

[21] F. Carella, L. Degli Esposti, A. Adamiano, M. Iafisco, The use of calcium phosphates in cosmetics, state of the art and future perspectives, Materials (Basel) 14 (2021) 6398, https://doi.org/10.3390/ma14216398.

[22] D.L. Slomberg, R. Catalano, V. Bartolomei, J. Labille, Release and fate of nanoparticulate TiO_2 UV filters from sunscreen: effects of particle coating and formulation type, Environ. Pollut. 271 (2021), 116263, https://doi.org/10.1016/J.ENVPOL.2020.116263.

[23] A. Rampaul, I.P. Parkin, L.P. Cramer, Damaging and protective properties of inorganic components of sunscreens applied to cultured human skin cells, J. Photochem. Photobiol. A Chem. 191 (2007) 138–148, https://doi.org/10.1016/J.JPHOTOCHEM.2007.04.014.

[24] N. Martin, B. Wassmur, D. Slomberg, J. Labille, T. Lammel, Influence of TiO_2 nanocomposite UV filter surface chemistry and their interactions with organic UV filters on uptake and toxicity toward cultured fish gill cells, Ecotoxicol. Environ. Saf. 243 (2022), 113984, https://doi.org/10.1016/J.ECOENV.2022.113984.

[25] J. Hu, L. Yang, P. Yang, S. Jiang, X. Liu, Y. Li, Polydopamine free radical scavengers, Biomater. Sci. 8 (2020) 4940–4950, https://doi.org/10.1039/d0bm01070g.

[26] A. Bino, A. Baldisserotto, E. Scalambra, V. Dissette, D.E. Vedaldi, A. Salvador, E. Durini, S. Manfredini, S. Vertuani, Design, synthesis and biological evaluation of novel hydroxy-phenyl-1H-benzimidazoles as radical scavengers and UV-protective agents, J. Enzym. Inhib. Med. Chem. 32 (2017) 527–537, https://doi.org/10.1080/14756366.2016.1265523.

[27] S.Q. Wang, Y. Balagula, U. Osterwalder, Photoprotection: a review of the current and future technologies, Dermatol. Ther. 23 (2010) 31–47, https://doi.org/10.1111/j.1529-8019.2009.01289.x.

[28] S.R. Ghazali, N.H. Rosli, L.S. Hassan, M.Z. Helmi Rozaini, H. Hamzah, Biocompatibility of hydroxyapatite (HAp) derived from clamshell as active ingredients in sunscreen product, in: IOP Conf. Ser. Earth Environ. Sci. 646, 2021, 012059, https://doi.org/10.1088/1755-1315/646/1/012059.

[29] A. Pal, K. Hadagalli, P. Bhat, V. Goel, S. Mandal, Hydroxyapatite—a promising sunscreen filter, J. Aust. Ceram. Soc. 56 (2020) 345–351, https://doi.org/10.1007/s41779-019-00354-2.

[30] A. Adamiano, F. Carella, L. Degli Esposti, C. Piccirillo, M. Iafisco, Calcium phosphates from fishery byproducts as a booster of the sun protection factor in sunscreens, ACS Biomater. Sci. Eng. 8 (2022) 4987–4995, https://doi.org/10.1021/acsbiomaterials.2c00680.

[31] F. Taraballi, S. Minardi, A. Kumar, F. Baino, S.S. Han, S. Kargozar, Additive manufacturing methods for producing hydroxyapatite and hydroxyapatite-based composite scaffolds: a review, Front. Mater. 6 (2019) 313, https://doi.org/10.3389/fmats.2019.00313.

[32] E. Campodoni, M. Montanari, C. Artusi, G. Bassi, F. Furlani, M. Montesi, S. Panseri, M. Sandri, A. Tampieri, Calcium-based biomineralization: a smart approach for the design of novel multifunctional hybrid materials, J. Compos. Sci. 5 (2021) 278, https://doi.org/10.3390/jcs5100278.

[33] A. Tampieri, T. D'Alessandro, M. Sandri, S. Sprio, E. Landi, L. Bertinetti, S. Panseri, G. Pepponi, J. Goettlicher, M. Bañobre-López, J. Rivas, Intrinsic magnetism and hyperthermia in bioactive Fe-doped hydroxyapatite, Acta Biomater. 8 (2012) 843–851, https://doi.org/10.1016/j.actbio.2011.09.032.

[34] E. Campodoni, Design and Development of Bio-hybrid Multifunctional Materials for Regenerative Medicine, University of Parma, 2018. https://hdl.handle.net/1889/3763.

[35] J. Liu, S. Yang, X. Li, Q. Yan, M.J.T. Reaney, Z. Jiang, Alginate oligosaccharides: production, biological activities, and potential applications, Compr. Rev. Food Sci. Food Saf. 18 (2019) 1859–1881, https://doi.org/10.1111/1541-4337.12494.

[36] D. Liu, M. Nikoo, G. Boran, P. Zhou, J.M. Regenstein, Collagen and gelatin, Annu. Rev. Food Sci. Technol. 6 (2015) 527–557, https://doi.org/10.1146/annurev-food-031414-111800.

[37] T. Yotsuyanagi, I. Yoshioka, N. Segi, K. Ikeda, Acid-induced and calcium-induced gelation of alginic acid: bead formation and pH-dependent swelling, Chem. Pharm. Bull. 39 (1991) 1072–1074, https://doi.org/10.1248/cpb.39.1072.

[38] A. Adamiano, N. Sangiorgi, S. Sprio, A. Ruffini, M. Sandri, A. Sanson, P. Gras, D. Grossin, C. Francès, K. Chatzipanagis, M. Bilton, B. Marzec, A. Varesano, F. Meldrum, R. Kröger, A. Tampieri, Biomineralization of a titanium-modified hydroxyapatite semiconductor on conductive wool fibers, J. Mater. Chem. B 5 (2017) 7608–7621, https://doi.org/10.1039/c7tb00211d.

[39] C. Menale, E. Campodoni, E. Palagano, S. Mantero, M. Erreni, A. Inforzato, E. Fontana, F. Schena, R. van't Hof, M. Sandri, A. Tampieri, A. Villa, C. Sobacchi, Mesenchymal stromal cell-seeded biomimetic scaffolds as a factory of soluble RANKL in Rankl-deficient osteopetrosis, Stem Cells Transl. Med. 8 (2019) 22–34, https://doi.org/10.1002/sctm.18-0085.

[40] E. Campodoni, S.M. Dozio, S. Panseri, M. Montesi, A. Tampieri, M. Sandri, Mimicking natural microenvironments: design of 3D-aligned hybrid scaffold for dentin regeneration, Front. Bioeng. Biotechnol. 8 (2020) 836, https://doi.org/10.3389/fbioe.2020.00836.

[41] X. Zhao, S. Ng, B.C. Heng, J. Guo, L. Ma, T.T.Y. Tan, K.W. Ng, S.C.J. Loo, Cytotoxicity of hydroxyapatite nanoparticles is shape and cell dependent, Arch. Toxicol. 87 (2013) 1037–1052, https://doi.org/10.1007/s00204-012-0827-1.

[42] European Commission, Scientific committee on consumer safety (SCCS), Sci. Committees. (2021) 1–81. https://ec.europa.eu/health/scientific_committees/consumer_safety_en.

[43] I.M. Joni, L. Nulhakim, C. Panatarani, Characteristics of TiO_2 particles prepared by simple solution method using $TiCl_3$ precursor, J. Phys. Conf. Ser. 1080 (2018), 012042, https://doi.org/10.1088/1742-6596/1080/1/012042.

[44] P.O. Kuzema, O.N. Stavinskaya, I.V. Laguta, O.A. Kazakova, Thermogravimetric study of water affinity of gelatin materials, J. Therm. Anal. Calorim. 122 (2015) 1231–1237, https://doi.org/10.1007/s10973-015-4823-6.

[45] J.P. Soares, J.E. Santos, G.O. Chierice, E.T.G. Cavalheiro, Thermal behavior of alginic acid and its sodium salt, Eclet. Quim. 29 (2004) 53–56, https://doi.org/10.1590/s0100-46702004000200009.

[46] E. Landi, A. Tampieri, M. Mattioli-Belmonte, G. Celotti, M. Sandri, A. Gigante, P. Fava, G. Biagini, Biomimetic Mg- and Mg,CO_3-substituted hydroxyapatites: synthesis characterization and in vitro behaviour, J. Eur. Ceram. Soc. 26 (2006) 2593–2601, https://doi.org/10.1016/J.JEURCERAMSOC.2005.06.040.

[47] C. Piccirillo, C. Rocha, D.M. Tobaldi, R.C. Pullar, J.A. Labrincha, M.O. Ferreira, P. M.L. Castro, M.M.E. Pintado, A hydroxyapatite-Fe_2O_3 based material of natural origin as an active sunscreen filter, J. Mater. Chem. B 2 (2014) 5999–6009, https://doi.org/10.1039/c4tb00984c.

[48] S. Smaoui, H. Ben Hlima, I. Ben Chobba, A. Kadri, Development and stability studies of sunscreen cream formulations containing three photo-protective filters, Arab. J. Chem. 10 (2017) S1216–S1222, https://doi.org/10.1016/j.arabjc.2013.02.020.

[49] A. Marucco, E. Carella, I. Fenoglio, A comparative study on the efficacy of different probes to predict the photo-activity of nano-titanium dioxide toward biomolecules, RSC Adv. 5 (2015) 89559–89568, https://doi.org/10.1039/c5ra14303a.

[50] I. Fenoglio, J. Ponti, E. Alloa, M. Ghiazza, I. Corazzari, R. Capomaccio, D. Rembges, S. Oliaro-Bosso, F. Rossi, Singlet oxygen plays a key role in the toxicity and DNA damage caused by nanometric TiO_2 in human keratinocytes, Nanoscale 5 (2013) 6567–6576, https://doi.org/10.1039/c3nr01191g.

[51] D.C. Hurum, A.G. Agrios, K.A. Gray, T. Rajh, M.C. Thurnauer, Explaining the enhanced photocatalytic activity of Degussa P25 mixed-phase TiO_2 using EPR, J. Phys. Chem. B 107 (2003) 4545–4549, https://doi.org/10.1021/jp0273934.

[52] Q. Feng, K. Wei, S. Lin, Z. Xu, Y. Sun, P. Shi, G. Li, L. Bian, Mechanically resilient, injectable, and bioadhesive supramolecular gelatin hydrogels crosslinked by weak host-guest interactions assist cell infiltration and in situ tissue regeneration, Biomaterials 101 (2016) 217–228, https://doi.org/10.1016/J.BIOMATERIALS.2016.05.043.

[53] A.D. Augst, H.J. Kong, D.J. Mooney, Alginate hydrogels as biomaterials, Macromol. Biosci. 6 (2006) 623–633, https://doi.org/10.1002/mabi.200600069.

[54] M.I. Neves, L. Moroni, C.C. Barrias, Modulating alginate hydrogels for improved biological performance as cellular 3D microenvironments, Front. Bioeng. Biotechnol. 8 (2020) 665, https://doi.org/10.3389/fbioe.2020.00665.
[55] M.B. Łabowska, K. Cierluk, A.M. Jankowska, J. Kulbacka, J. Detyna, I. Michalak, A review on the adaption of alginate-gelatin hydrogels for 3D cultures and bioprinting, Materials (Basel) 14 (2021) 1–28, https://doi.org/10.3390/ma14040858.
[56] K. Anselme, Osteoblast adhesion on biomaterials, Biomaterials. 21 (2000) 667–681, https://doi.org/10.1016/S0142-9612(99)00242-2.